C.; Nakatani, K.	Gold Nanoparticle Assembly by Turning On and Off DNA Hybridization with Thermally Degradable Molecular Glue	*Chem*		485	
Takei, F.; Suda, H.; Hagihara, M.; Zhang, J.; Kobori, A.; Nakatani, K.	Allele Specific C-Bulge Probes with One Unique Fluorescent Molecule Discriminate the Single Nucleotide Polymorphism in DNA	*Chem. Eur. J.*	*in press*		**2007**
Li, X.; Song, H.; Nakatani, K.; Kraatz, H.-B.	Exploiting Small Molecule Binding to DNA for the Detection of Single-Nucleotide Mismatches and Their Base Environment	*Anal. Chem.*	*79*	2552-2555	**2007**
Goto, Y.; Hagihara, S.; Hagihara, M.; Nakatani, K.	Small molecule binding to non-Quadruplex form of the Human Telomeric Sequence	*ChemBio Chem*	*in press*		**2007**
Dohno, C.; Nakatani, K.	Control of DNA hybridization by photoswitchable mismatch binding ligands.	*Nucleic Acids Symp. Ser.*	*50*	87-88	**2006**
Hagihara, M.; Nakatani, K.	Inhibition of DNA replication by a d(CAG) repeat binding ligand	*Nucleic Acids Symp. Ser.*	*50*	147-148	**2006**
Tanaka, Y.;	Nature of the Chemical	*J. Am.*	*126*	744-	**2004**

Kasai, Y.; Mochizuki, S.; Wakisaka, A.; Morita, E. H.; Kojima, C.; Toyozawa, A.; Kondo, Y.; Taki, M.; Takagi, Y.; Inoue, A.; Yamasaki, K.; Taira, K.	Bond Formed with the structural Metal Ion at the A9G10.1 Motif Derived from Hammerhead Ribozymes	*Chem. Soc.*		752	
Fujiwara, K.; Tenno, T.; Sugasawa, K.; Jee, J. G.; Ohki, I.; Kojima, C.; Tochio, H.; Hiroaki, H.; Hanaoka, F.; Shirakawa, M.	Structure of the ubiquitin-interacting motif of S5a bound to the ubiquitin-like domain of HR23B	*J. Biol. Chem.*	*279*	4760-4767	**2004**
Nomura, M.; Kobayashi, T.; Kohno, T.; Fujiwara, K.; Tenno, T.; Shirakawa, M.; Ishizaki, I.; Yamamoto, K.; Matsuyama, T.; Mishima, M.; Kojima, C.	Paramagnetic NMR study of Cu2+-IDA complex localization on a protein surface and its application to elucidate long distance information	*FEBS Lett.*	*566*	157-161	**2004**
Ishizaki, I.;	Solution NMR study of	*Nucleic*	*4*	105–	**2004**

Nomura, M.; Yamamoto, K.; Matsuyama, T.; Mishima, M.; Kojima, C.	DNA recognition mechanism of IRF4 protein	*Acids Res. Suppl.*		106	
Kobayashi, T.; Mishima, M.; Akagi, K.; Sakai, N.; Katoh, E.; Takano, M.; Yamazaki, T.; Kojima, C.	^{1}H, ^{15}N and ^{13}C backbone and side-chain assignments of the rice phytochrome B PAS1 domain and backbone assignments of the PAS1-PAS2 domain	*J. Biomol. NMR*	*31*	269-270	**2005**
Sudo, Y.; Okuda, H.; Yamabi, M.; Fukuzaki, Y.; Mishima, M.; Kamo, N.; Kojima, C.	Linker region of a Halobacterial transducer protein interacts directly with its sensor retinal protein	*Biochemistry*	*44*	6144-6152	**2005**
Mishima, M.; Shida, T.; Yabuki, K.; Kato, K.; Sekiguchi, J.; Kojima, C.	Solution structure of the peptidoglycan binding domain of B. subtilis cell wall lyticenzyme CwlC: Characterization of the sporulation-related repeats by NMR	*Biochemistry*	*44*	10153-10163	**2005**
Iida, E.; Satou, K.; Mishima, M.; Kojima, C.; Harashima, H.; Kamiya, H.	Amino acid residues involved in substrate recognition of the *Escherichia coli* ORF135 protein	*Biochemistry*	*44*	5683-5689	**2005**

Kubo, M.; Sato, M.; Aizawa, T.; Kojima, C.; Kamo, N.; Mizuguchi, M.; Kawano, K.; Demura, M.	Disassembling and bleaching of chloride-free pharaonis halorhodopsin by octyl-beta-glucoside	*Biochemistry*	*44*	12923-12931	**2005**
Yoshida, K.; Yamamoto, K.; Kohno, T.; Hironaka, N.; Yasui, K.; Kojima, C.; Mukae, H.; Kadota, J.; Suzuki, S.; Honma, K.; Kohno, S.; Matsuyama, T.	Active Repression of IFN Regulatory Factor-1-Mediated Transactivation by IFN Regulatory Factor-4	*Int. Immunol.*	*17*	1463-1471	**2005**
Nakatani, K.; Hagihara, S.; Goto, Y.; Kobori, A.; Hagihara, M.; Hayashi, G.; Kyo, M.; Nomura, M.; Mishima, M.; Kojima, C.	Solution structure of a small-molecular ligand complexed with CAG trinucleotide repeat DNA	*Nucleic Acids Res. Suppl.*	*5*	49-50	**2005**
Tanaka, Y.; Yamaguchi, H.; Oda, S.; Kojima, C.; Ono, A.;	NMR spectroscopic analyses of functional nucleic acids-metal interaction and their	*Nucleic Acids Res. Suppl.*	*5*	51-52	**2005**

Taira, K.; Kondo, Y.	solution structure analyses				
Yamaguchi, H.; Oda, S.; Kojima, C.; Ono, A.; Kondo, Y.; Tanaka, Y.	Spectroscopic analyses of DNA duplexes in the presence of mercury ions	*Nucleic Acids Res. Suppl.*	*5*	199-200	**2005**
Nomura, M.; Hagihara, S.; Goto, Y.; Nakatani, K.; Kojima, C.	NMR structural analysis of the G.G Mismatch DNA complexed with Naphthyridine-Dimer	*Nucleic Acids Res. Suppl.*	*5*	213-214	**2005**
Tanaka, Y.; Yamaguchi, H.; Oda, S.; Kondo, Y.; Nomura, M.; Kojima, C.; Ono, A.	NMR spectroscopic study of a DNA duplex with mercury-mediated T-T basepairs	*Nucleosides Nucleotides Nucleic Acids*	*25*	613-624	**2006**
Furuita, K.; Mishima, M.; Kojima, C.	^{1}H, ^{13}C and ^{15}N resonance assignments of the VAP-A: OSBP complex	*J. Biomol. NMR*	*36 Supp 1 5*	69	**2006**
Tanaka, Y.; Oda, S.; Yamaguchi, H.; Kudo, M.; Kondo, Y.; Kojima, C.; Ono, A.	Structural analyses on the mercury^{II}- mediated T-T base pair	*Nucleic Acids Symp. Ser.*	*50*	47-48	**2006**
Furuita, K.; Ishizaki, I.; Fukada, H.;	Studies of DNA recognition mechanism of transcription factor	*Nucleic Acids Symp.*	*50*	259-261	**2006**

Yamamoto, K.; Matsuyama, T.; Nomura, M.; Mishima, M.; Kojima, C.	IRF-4	*Ser.*			
Tanaka, Y.; Oda, S.; Yamaguchi, H.; Kondo, Y.; Kojima, C.; Ono , A.	^{15}N-^{15}N *J*-coupling across Hg^{II}: Direct observation of Hg^{II}-mediated T-T base pairs in a DNA duplex	*J. Am. Chem. Soc.*	*129*	244-245	**2007**
Mishima, M.; Wakabayashi, S.; Kojima, C.	Solution structure of the cytoplasmic region of Na^+/H^+ exchanger 1 complexed with essential cofactor calcineurin B homologous protein 1	*J. Biol. Chem.*	*282*	2741-2751	**2007**

研究成果の刊行物

J|A|C|S
ARTICLES
Published on Web 12/19/2003

The SPR Sensor Detecting Cytosine−Cytosine Mismatches

Akio Kobori,† Souta Horie,‡ Hitoshi Suda,‡ Isao Saito,‡ and Kazuhiko Nakatani*,†,‡

Contribution from the Department of Synthetic Chemistry and Biological Chemistry, Faculty of Engineering, Kyoto University, Kyoto 615-8510, Japan, and PRESTO, Japan Science and Technology Agency (JST), Kyoto 615-8510, Japan

Received August 15, 2003; E-mail: nakatani@sbchem.kyoto-u.ac.jp

Abstract: We have synthesized the first surface plasmon resonance (SPR) sensor that detects cytosine−cytosine (C−C) mismatches in duplex DNA by immobilizing aminonaphthyridine dimer on the gold surface. The ligand consisting of two 2-aminonaphthyridine chromophores and an alkyl linker connecting them strongly stabilized the C−C mismatches regardless of the flanking sequences. The fully matched duplexes were not stabilized at all under the same conditions. The C−T, C−A, and T−T mismatches were also stabilized with a reduced efficiency. SPR analyses of mismatch-containing 27-mer duplexes were performed with the sensor surface on which the aminonaphthyridine dimer was immobilized. The response for the C−C mismatch in 5′-GCC-3′/3′-CCG-5′ was about 83 times stronger than that obtained for the fully matched duplex. The sensor successfully detects the C−C mismatch at the concentration of 10 nM. SPR responses are proportional to the concentration of the C−C mismatch in a range up to 200 nM. Aminonaphthyridine dimer could bind strongly to the C−C mismatches having 10 possible flanking sequences with association constants in the order of 10^6 M^{-1}. The facile protonation of 2-aminonaphthyridine chromophore at pH 7 producing the hydrogen-bonding surface complementary to that of cytosine was most likely due to the remarkably high selectivity of **1** to the C−C mismatch.

Introduction

Surface plasmon resonance (SPR) detects changes in the refractive index caused by variation of the mass on the sensor chip surface, e.g., when the analyte binds to the immobilized ligand on the surface.[1] In most SPR studies, macromolecules such as proteins and DNAs are immobilized on the sensor surface to detect protein−protein[2,3] and protein−DNA[4,5] interactions. We have studied the SPR detection of mismatched base pairs by using the sensor surface where a small molecular weight ligand that specifically binds to the mismatched base pairs was immobilized.[6−10] This technique would be useful for the high-throughput heteroduplex analyses of single nucleotide polymorphisms (SNP). Heteroduplex analyses[11,12] detect the mismatched base pairs in heteroduplexes produced by cross-hybridization of a sample and the standard DNAs.[13−15] When a sample DNA is identical to the standard DNA in base sequences, cross-hybridization of two DNAs produces a fully matched duplex but not a heteroduplex containing a mismatch site. Therefore, the heteroduplex analyses need analytical methods that discriminate the mismatch-containing duplexes from the fully matched duplexes. Conventional low-throughput methods for the detection of mismatched base pairs in heteroduplex analyses were enzymatic and chemical cleavage at the mismatched sites,[16−18] gel electrophoresis,[12,19] and selective capture by mismatch-binding proteins.[20,21] Heteroduplex analyses are applicable to both SNP discovery (mapping) and detection (typing). In the SNP mapping, mismatched base pairs produced in a heteroduplex will be identified by the subsequent sequencing. In contrast, a predetermined mismatched base pair is produced in SNP detection because the sequence of the standard DNA, the site of mutation, and the type of mutation have been identified. We report here the first SPR sensor detecting C−C mismatches in duplex DNA on which novel ligand molecule aminonaphthyridine dimer **1** was immobilized on the surface. The ligand strongly stabilized the C−C

† PRESTO, Japan Science and Technology Agency.
‡ Kyoto University.

(1) *Biacore User's Manual*; Pharmacia-Biosensor: Piscatway, NJ, 1990.
(2) Williams, C. *Curr. Opin. Biotechnol.* **2000**, *11*, 42−46.
(3) Quinn, J. G.; O'Neill, S.; Doyle, A.; McAtamney, C.; Diamond, D.; MacCraith, B. D.; O'Kennedy, R. *Anal. Biochem.* **2000**, *281*, 135−143.
(4) Jayarajah, C. N.; Thompson, M. *Biosens. Bioelectron.* **2002**, *17*, 159−171.
(5) Willis, R. C. *Mod. Drug Discovery* **2002**, *5*, 26−33.
(6) Nakatani, K.; Sando, S.; Saito, I. *Nat. Biotechnol.* **2001**, *19*, 51−55.
(7) Nakatani, K.; Sando, S.; Kumasawa, H.; Kikuchi, J.; Saito, I. *J. Am. Chem. Soc.* **2001**, *123*, 12650−12657.
(8) Nakatani, K.; Sando, S.; Saito, I. *Bioorg. Med. Chem.* **2001**, *9*, 2381−2385.
(9) Smith, E. A.; Kyo, M.; Kumasawa, H.; Nakatani, K.; Saito, I.; Corn, R. M. *J. Am. Chem. Soc.* **2002**, *124*, 6810−6811.
(10) Nakatani, K.; Hagihara, S.; Sando, S.; Sakamoto, S.; Yamaguchi, K.; Maesawa, C.; Saito, I. *J. Am. Chem. Soc.* **2003**, *125*, 662−666.
(11) Landers, J. P. *Anal. Chem.* **2003**, *75*, 2919−2927.
(12) Nataraj, A. J.; Olivos-Glander, I.; Kusukawa, N. *Electrophoresis* **1999**, *20*, 1177−1185.
(13) Syvänen, A.-C. *Nat. Rev. Genet.* **2001**, *2*, 930−942.
(14) Kwok, P. Y. *Annu. Rev. Genomics Hum. Genet.* **2001**, *2*, 235−258.
(15) Schafer, A. J.; Hawkins, J. R. *Nat. Biotechnol.* **1998**, *16*, 33−39.
(16) Myers, R. M.; Larin, Z.; Maniatis, T. *Science* **1985**, *230*, 1242−1246.
(17) Rowley, G.; Saad, S.; Giannelli, F.; Green, P. M. *Genomics* **1995**, *30*, 574−582.
(18) Roberts, E.; Deeble, V. J.; Woods, C. G.; Taylor, G. R. *Nucleic Acids Res.* **1997**, *25*, 3377−3378.
(19) White, M. B.; Carvalho, M.; Derse, D.; O'Brien, S. J.; Dean, M. *Genomics* **1992**, *12*, 301−306.
(20) Fazakerley, G. V.; Qignard, E.; Woisard, A.; Guschlbauer, W.; van der Marel, G. A.; van Boom, J. H.; Jones, M.; Radman, M. *EMBO J.* **1986**, *5*, 3697−3703.
(21) Smith, J.; Modrich, P. *Proc. Natl. Acad. Sci. U.S.A.* **1996**, *93*, 4374−4379.

10.1021/ja037947w CCC: $27.50

Scheme 1. Synthesis of Aminonaphthyridine Derivatives[a]

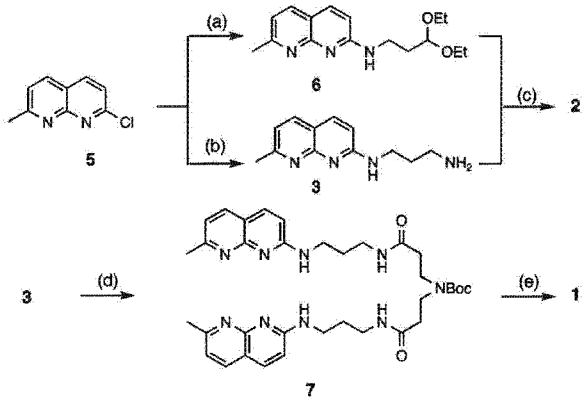

[a] Reagents and conditions: (a) 3,3-diethoxypropylamine, 81%; (b) diaminopropane, 95%; (c) (i) 80% AcOH, 80 °C, 30 min, (ii) $NaBH_3CN$, Et_3N, MeOH, 5 h, 12%; (d) 3,3-iminobis(pentafluorophenyl propionate), 67%; (e) 4 N HCl/ethyl acetate, 80%.

mismatches regardless of the flanking sequences as determined by the increase in melting temperatures (T_m). The **1**-immobilized sensor detected 27-mer duplex containing a C−C mismatch at the 10 nM concentration. Most genetic diseases are caused by the interaction of many genetic factors (polygenic) but not caused by a single genetic disorder (monogenic). It is anticipated that a large number of SNP sites must be determined for diagnoses of genetic diseases in the future. While G to C (or C to G) mutation producing a C−C mismatch in heteroduplex analyses is not high in frequency, under such situations, typing of G to C (or C to G) mutation would be indispensable.

Synthesis of Aminonaphthyridine Derivatives. A series of aminonaphthyridine derivatives **1**−**3** were synthesized as shown in Scheme 1. Substitution of chloride in 2-chloro-7-methyl-1,8-naphthyridine (**5**)[22] with diaminobutane and 3,3-diethoxypropylamine leads to amine **3** and diethylacetal **6**, respectively. Aminonaphthyridine dimer **2**, having the same linker length as that of acylaminonaphthyridine dimer **4**,[6,7] was obtained by a reductive coupling of **3** and **6**. Thus, the aldehyde derived from **6** by acid hydrolysis was treated with **3** under conditions of a reductive amination. Condensation of 3,3-iminobis(pentafluorophenyl propionate) with **3** afforded Boc-protected aminonaphthyridine dimer **7**. Finally, the amine-protecting Boc group of **7** was removed with 4 N HCl to give **1**.

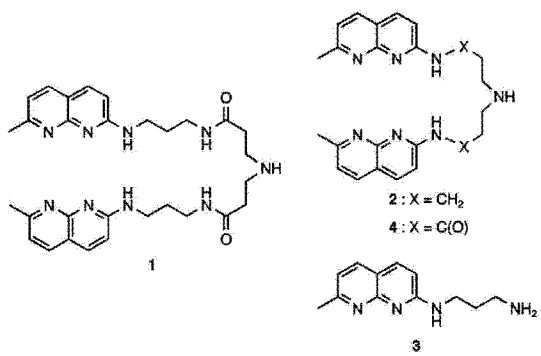

Preparation of Aminonaphthyridine Dimer-Immobilized Sensor. A synthetic scheme of **1**-immobilized sensor surface was shown in Scheme 2. Aminoalkyl linker was attached to **1** by a reductive amination with 4-((*tert*-butoxy)carbonylamino)-

Scheme 2. Preparation of Aminonaphthyridine Dimer-Immobilized Surface[a]

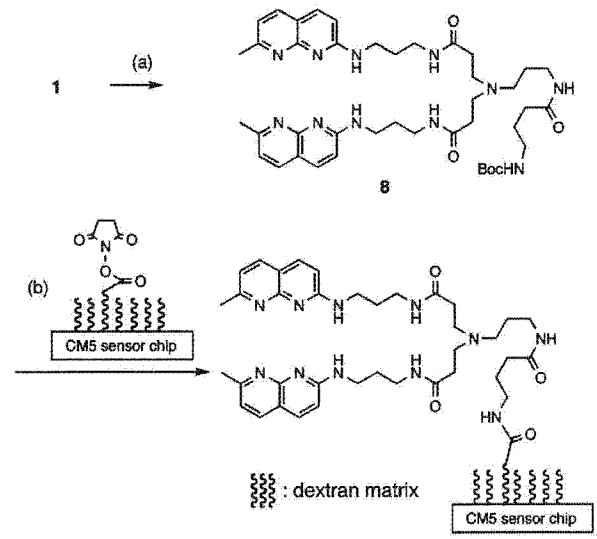

[a] Reagents and conditions: (a) 4-((*tert*-butoxy)carbonylamino)- *N*-(3-oxopropyl)butanamide, $NaBH_3CN$, AcOH, MeOH, 1 h, 95%; (b) (i) 4 N HCl/ethyl acetate, 30 min, (ii) amine coupling kit.

N-(3-oxopropyl)butanamide to give **8**. Following the deprotection of the Boc group of **8** with 4 N HCl, the resulting amine was coupled to the activated carboxylic acid of the CM5 sensor chip using a standard procedure of an amine coupling method.[23] The degree of immobilization of the ligands was monitored by the increasing SPR signal and controlled by changing the reaction time. After immobilization of the ligand, the activated esters that remained intact on the surface were destroyed by being treated with ethanol amine.

Melting Temperature of Mismatches in the Presence of Aminonaphthyridine Derivatives. Aminonaphthyridine dimer **1** consisted of two chromophores of 2-amino-7-methyl-1,8-naphthyridine and an alkyl linker connecting the exocyclic amino group of each chromophore. The molecule was discovered by a straightforward screening using increases of T_m of the mismatch-containing duplex DNA as an index. The UV melting curves of 11-mer duplexes of 5′-d(CTA AGX CAA TG)-3′/3′-d(GAT TCY GTT AC)-5′, where **X**−**Y** are any nucleotide combinations, were measured in the presence of **1** in sodium phosphate buffer (10 mM, pH = 7.0). The difference in the melting temperature (ΔT_m) in the absence and presence of **1** (100 μM) was summarized in Table 1.

The remarkable increase of T_m by 18.0 °C was observed for the C−C mismatch, whereas the T_m values of fully matched duplexes were not increased at all under the same conditions. Increases in T_m by 11.3, 7.2, and 4.0 °C were observed for C−T, T−T, and C−A mismatches, respectively. Other mismatches, including A−A, G−T, G−A, and G−G, showed little increase of their T_m values. These results indicated that aminonaphthyridine dimer **1** strongly stabilized the C−C mismatch and the mismatches containing a cytosine or thymine with a reduced efficiency. The extraordinary high selectivity of **1** to pyrimidine-containing mismatches was remarkable.

(22) Brown, E. V. *J. Org. Chem.* **1965**, *30*, 1607−1610.
(23) Löfås, S.; Johnson, B. *J. Chem. Soc., Chem. Commun.* **1990**, *21*, 1526−1528.

Table 1. ΔT_m Values for the 11-mer Duplexes Containing a Mismatch[a]

5′-CTAAGXCAATG-3′
3′-GATTCYGTTAC-5′

X–Y	T_m[b]	ΔT_m 1[c]	ΔT_m 2[c]	ΔT_m 3[d]
C–C	18.0 (0.4)	18.0 (0.4)	14.0 (0.7)	12.4 (0.8)
C–T	22.3 (0.5)	11.3 (0.3)	8.7 (0.1)	6.5 (0.8)
T–T	23.0 (0.8)	7.2 (0.6)	6.0 (0.6)	3.6 (1.2)
C–A	27.6 (0.4)	4.0 (0.1)	1.6 (0.2)	1.4 (0.6)
A–A	24.2 (0.4)	1.8 (0.8)	2.0 (0.5)	0.9 (0.3)
G–T	29.8 (0.2)	0.5 (0.7)	1.4 (0.2)	0.3 (0.0)
G–A	32.6 (0.6)	0.3 (0.8)	0.8 (0.7)	0.1 (1.1)
G–G	36.1 (0.5)	−0.1 (1.0)	0.3 (0.4)	−0.2 (1.0)
A–T	37.0 (0.3)	−0.1 (0.1)	0.0 (0.4)	0.0 (0.3)
C–G	43.1 (0.2)	−0.3 (0.5)	0.3 (0.3)	0.2 (0.4)

[a] T_m values of duplexes (4.5 μM) were measured in 10 mM sodium phosphate buffer (pH 7.0) containing 100 mM NaCl. All measurements were taken three times, and standard deviations are shown in parentheses. [b] T_m values of oligomers. [c] The concentration of **1** and **2** was 100 μM.[d] The concentration of **3** was 200 μM.

Table 2. ΔT_m Values for the 13-mer Duplexes Containing a C–C Mismatch in Different Flanking Sequences[a]

5′-GCTAA**xCz**AATGA-3′
3′-CGATT**yCw**TTACT-5′

5′-xCz-3′/3′-yCw-5′	T_m	ΔT_m
gCc/cCg	25.4 (0.3)	17.9 (0.6)
gCt/cCa	23.9 (0.3)	15.7 (0.2)
cCc/gCg	22.3 (0.3)	15.3 (0.7)
gCa/cCt	26.2 (0.4)	15.0 (0.5)
aCt/tCa	20.7 (0.4)	14.2 (0.4)
aCa/tCt	23.2 (0.3)	13.5 (0.1)
cCt/gCa	25.3 (0.1)	13.2 (0.2)
tCa/aCt	24.8 (0.5)	12.2 (0.7)
cCa/gCt	29.0 (0.1)	11.2 (0.3)
cCg/gCc	32.6 (0.2)	10.4 (0.2)

[a] Conditions of T_m measurements were the same as those in Table 1.

Aminonaphthyridine dimer **2**, where two naphthyridine chromophores were connected with a short alkyl linker compared with that in **1**, and monomer **3** were examined as reference molecules. The ΔT_m values obtained for the C–C mismatch in the presence of **2** (100 μM) and **3** (200 μM) were 14.0 and 12.4 °C, respectively. A decreased ΔT_m by 4.0 °C showed the significance of the linker structure on the stabilization of the mismatch. A much-reduced stabilization of the C–C mismatch by **3** showed that a covalent connection of two aminonaphthyridines is in fact effective.

Effects of sequences flanking to the C–C mismatch on the **1**-binding were examined with 13-mer duplex 5′-d(GCTAA **xCz** AATGA)-3′/3′-d(CGATT **yCw** TTACT)-5′ containing a C–C mismatch in the sequence of 5′-**xCz**-3′/3′-**yCw**-5′, where **x**–**y** and **z**–**w** were any combination of Watson–Crick base pairs. The ΔT_m values obtained for all sequences were over 10 °C, indicating that **1** could stabilize the C–C mismatches regardless of the flanking sequences (Table 2). Rather low ΔT_m values of 10.4 and 11.2 °C recorded for **cCg/gCc** and **cCa/gCt** were due to the high T_m values of the duplex.[24]

Evaluation of Aminonaphthyridine-Immobilized Sensor. Having discovered that **1** strongly stabilized the C–C mismatches, we synthesized SPR chips for the C–C mismatch detection by immobilizing **1** on the sensor surface. SPR analyses of mismatch-containing 27-mer 5′-d(GTT ACA GAA TCT GXC AAG CCT AAT ACG)-3′/3′-d(CAA TGT TTC AGA CYG TTC GGA TTA TGC)-5′ were performed with **1**-immobilized sensor surface (for 810 response units (RU)) at pH 7.0. A marked SPR response was obtained for the duplex containing the C–C mismatch at the DNA concentration of 200 nM (Figure 1a). The response at 180 s after an injection of DNA was 399 RU, about 83 times stronger than that obtained for the fully matched duplex (4.8 RU). The duplex containing a C–T mismatch produced an intermediate response (80 RU). As shown in Figure 1b, SPR responses of the C–A and T–T mismatches were weak (19 and 9 RU, respectively) but distinguishable from that of the fully matched duplex. SPR responses of other mismatches were indistinguishable from the fully matched duplex (data not shown). These results were consistent with the ΔT_m of the mismatches in the presence of **1** (cf. Table 1). To further evaluate the novel SPR sensor, the detection limit of the C–C mismatch and the concentration dependency of SPR responses were examined. The sensor surface where **1** was immobilized for 955 RU successfully detected the C–C mismatch at the 10 nM concentration (Figure 1c). Further lowering the concentration of the C–C mismatch resulted in a loss of signals. By using aminonaphthyridine dimer **1** and the Biacore 2000 equipment, a concentration of 10 nM for the 27-mer duplex was found to be the lower limit for the detection of the C–C mismatch. Because the SPR intensity increased with increasing molecular weight of the analyte, the detection limit of longer duplexes containing the C–C mismatch would be

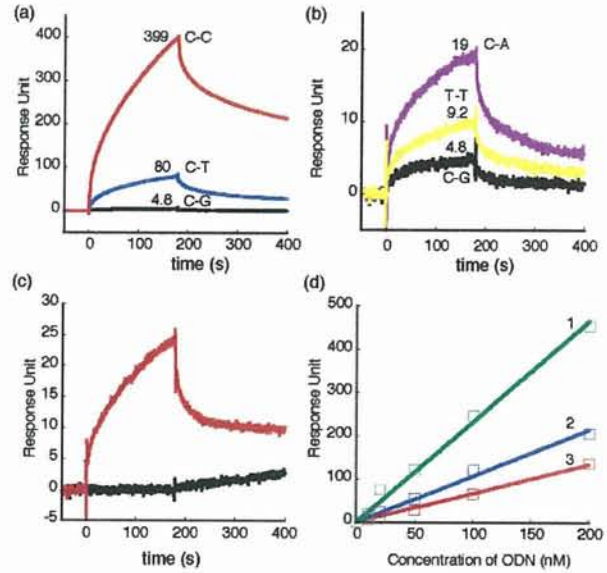

Figure 1. (a) and (b) SPR assay of 27-mer duplex (**GXC/CYG**) (0.2 μM) containing C–C (**GCC/CCG**) (red), C–T (**GCC/CTG**) (blue), C–A (**GCC/CAG**) (purple), and T–T (**GTC/CTG**) (yellow) mismatches and CG (**GCC/CGG**) match (black) with the **1**-immobilized sensor surface. Binding was measured for 180 s and dissociation for 220 s in a phosphate buffer (200 mM, pH 7.0) containing NaCl (150 mM). (c) SPR assay of C–C mismatch (red) and C–G match (black) at 10 nM. (d) Concentration dependency for the SPR response of the C–C mismatch (0–200 nM). The response after 100 s of association time was plotted against the DNA concentration. Experimental data obtained with the surface where **1** was immobilized for (1) 955 RU (green square), (2) 506 RU (blue square), and (3) 434 RU (red squares) were overlaid with a linear fitted line.

(24) For discussions on the relationship between ΔT_m and the binding affinity, see: (a) Nakatani, K.; Horie, S.; Saito, I. *Bioorg. Med. Chem.* **2003**, *19*, 51–55. (b) Peyret, N.; Seneviratne, P. A.; Allawi, H. T.; SantaLucia, J., Jr. *Biochemistry* **1999**, *38*, 3468–3477.

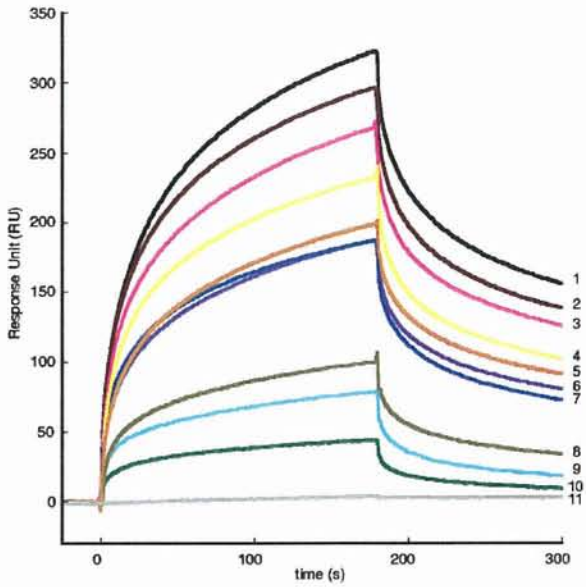

Figure 2. SPR sensorgrams were obtained by analyzing 27-mer 5′-d(GTT ACA GAA TCT **XCZ** AAG CCT AAT ACG)-3′/3′-d(CAA TGT CTT AGA **YCW** TTC GGA TTA TGC)-5′ containing all kinds of flanking sequences. Binding to **1**-immobilized sensor where **1** was immobilized for 380 RU was measured in a phosphate buffer (200 mM, pH 7.0) containing NaCl (150 mM). Key: (1) **GCC/CCG**, (2) **GCT/CCA**, (3) **CCC/GCG**, (4) **CCT/GCA**, (5) **CCG/GCC**, (6) **GCA/TCA**, (7) **ACT/TCA**, (8) **CCA/GCT**, (9) **TCT/ACA**, (10) **TCA/ACT**, and (11) **GCC/CGG**.

below 10 nM. SPR responses of the C−C mismatch obtained by three sensors containing different amounts of immobilized **1** are proportional to the concentration of the C−C mismatch in a range up to 200 nM (Figure 1d). These observations validate that the observed SPR responses are in fact due to the interaction between **1** on the surface and the C−C mismatched DNA.

Thermodynamics for the binding of the C−C mismatches to the aminonaphthyridine dimer-immobilized surface were investigated with regard to the effect of the flanking sequence to the mismatch. Sensorgrams of 27-mer 5′-d(GTT ACA GAA TCT **XCZ** AAG CCT AAT ACG)-3′/3′-d(CAA TGT CTT AGA **YCW** TTC GGA TTA TGC)-5′ containing all kinds of flanking sequences (5′-**XCZ**-3′/3′-**YCW**-5′) were clearly distinguishable from that of the fully matched duplex (Figure 2). The response obtained for **GCC/CCG** where the mismatch was flanked by two G−C base pairs was 323 RU at 180 s. A 7-fold decrease in response was observed by replacing the two G−C base pairs with two A−T base pairs in **TCA/ACT** (44.2 RU). However, the response to **TCA/ACT** was about 10-fold larger than that to the fully matched duplex. The order of magnitude in SPR response was consistent with that in ΔT_m with different flanking sequences (cf. Table 2). Association constants (K_a) of **1** to the C−C mismatches were estimated by fitting the sensorgrams to a 1:1 Langmuir model with BIAevaluation software (version 3) (Table 3). The largest K_a of 7.8×10^6 M^{-1} was obtained for **GCC/CCG**, whereas the smallest K_a of 1.5×10^6 M^{-1} was obtained for **TCA/ACT**. These data demonstrated that the binding of **1** to the C−C mismatches was stronger for those flanking G−C base pairs than those flanking A−T base pairs. This is rationalized by an improved stacking stabilization of the complex by the flanking G−C base pairs compared to that by the A−T base pairs.[25,26]

Table 3. Association Constants for **1**-Binding to C−C Mismatches[a]

5′-XCZ-3′/3′-YCW-5′	K_a (10^6 M^{-1})
GCC/CCG	7.8
GCT/CCA	6.9
CCC/GCG	7.3
CCT/GCA	6.1
CCG/GCC	5.3
GCA/CCT	5.0
ACT/TCA	4.5
CCA/GCT	3.0
TCT/ACA	1.7
TCA/ACT	1.5

[a] Association constants for the binding of **1** to 27-mer 5′-d(GTT ACA GAA TCT **XCZ** AAG CCT AAT ACG)-3′/3′-d(CAA TGT CTT AGA **YCW** TTC GGA TTA TGC)-5′ were estimated by fitting the sensorgrams (Figure 2) to a 1:1 Langmuir model with BIAevaluation software, version 3.

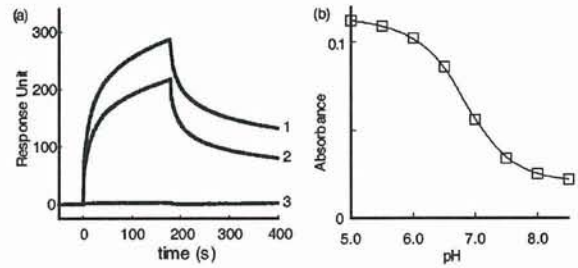

Figure 3. (a) SPR sensorgrams for the binding of 27-mer duplex (**GCC/CCG**) (1.0 μM) containing a C−C mismatch to the **1**-immobilized sensor surface. Binding was measured in a phosphate buffer (200 mM) containing NaCl (150 mM) at (1) pH 6.0, (2) pH 7.0, and (3) pH 8.0. (b) pH dependency of a UV absorbance of **3** at 370 nm. UV absorbance was measured in 10 mM sodium phosphate buffer in the presence of **3** (10 μM) at various pH conditions.

Model of Base Pairing between Aminonaphthyridine. We have reported that the structurally closely related compound **4**, where exocyclic amino groups in two 2-amino-7-methyl-1,8-naphthyridines were connected by an amide linkage, strongly stabilized the G−G mismatch but not the C−C mismatch at all.[6,7,27] Since both **2** and **4** have the same hydrogen-bonding surface complementary to guanine but not to cytosine, the striking differences in base selectivity between **2** and **4** need rational explanations. It was found that SPR response of the **1**-immobilized surface was sensitive to the pH of the buffer. A strong binding of 27-mer duplex (1.0 μM) containing a C−C mismatch with the **1**-immobilized sensor surface was observed at pH 6.0 and 7.0, whereas little binding was detected at pH 8.0 (Figure 3a). The responses at pH 6.0, 7.0, and 8.0 at 180 s after injection of 27-mer were 287, 216, and 2.7 RU, respectively. These results showed that the binding of aminonaphthyridine to a cytosine is dramatically suppressed at pH 8.0. The pH dependency of the UV absorbance of **3** revealed that the pK_a of the protonated **3** is about 6.8, showing that about 40% of the 2-aminonaphthyridine chromophore in **1**, **2**, and **3** in a free state would be protonated at pH 7.0 (Figure 3b). Protonation of the chromophore at the N1 position modulates from the hydrogen-bonding surface complementary to guanine to that to cytosine (Figure 4a). It is reasonable to estimate that

(25) Sponer, J.; Leszczynski, J.; Hobza, P. *J. Phys. Chem.* **1996**, *100*, 5591−5596.
(26) Alhambra, C.; Luque, F. J.; Gago, F.; Orozco, M. *J. Phys. Chem.* **1997**, *101*, 3846−3853.
(27) Murray, T. J.; Zimmerman, S. C. *J. Am. Chem. Soc.* **1992**, *114*, 4010−4011.

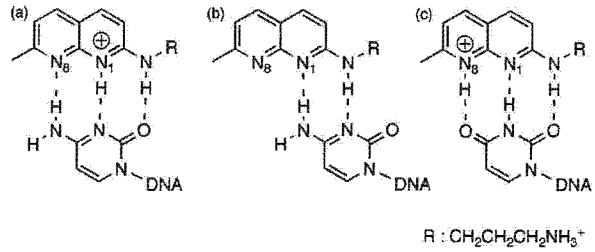

Figure 4. Proposed models of base-pairing between (a) cytosine and N1-protonated **3**, (b) cytosine and **3**, and (c) thymine and N8-protonated **3**.

the protonation of N1 in a bound state of 2-aminonaphthyridine to cytosine at neutral pH would be more facile than the protonation in a free state. While hydrogen bonding between nonprotonated aminonaphthyridine and cytosine is feasible through two hydrogen bonds (Figure 4b), energy gain by the hydrogen bonding calculated at the B3LYP/6-31G** level was 6.9 kcal/mol smaller than that between 1-methylcytosine and N1-protonated 2-methylamino-7-methylnaphthyridine.[28,29] On the basis of these arguments, the remarkably high selectivity of **1** to the C–C mismatch is most likely due to a facile protonation of the chromophore under neutral pH.

The presence of a carbonyl group next to the exocyclic amino group in 2-aminonaphthyridine is responsible for the remarkable difference in binding selectivity to the mismatch. The strength of a hydrogen bond is related to the hydrogen-bonding acidity of the donor group involved.[30,31] Beijer et al. have reported that the association constant of the complex of 2,6-diaminopyridine with *N*-propylthymine increases approximately 10-fold upon acylation of the amino groups.[32,33] It is highly likely that an acylation of the exocyclic amino group of 2-aminonaphthyridine significantly improves the stability of the hydrogen-bonding pair to a guanine. Since the acylated aminonaphthyridine is less susceptible to the protonation at N1 and N8, the dimer of acylated naphthyridine showed negligible binding to the C–C mismatch.

Protonation of 2-amino-1,8-naphthyridine is feasible both at N1 and N8 positions. While N1 protonation produces the hydrogen-bonding surface that is complementary to that of cytosine as discussed above, N8 protonation produces a surface complementary to that of thymine (Figure 4c). This is most likely the molecular basis for the binding of **1** to the C–T mismatch. The decreased binding to the C–T mismatch compared to the binding to the C–C mismatch was rationalized by an unfavorable secondary interaction in the hydrogen-bonded complex with alternating donor (D) and acceptor (A) groups. Studies on secondary interaction in a triple hydrogen-bonded complex by Jorgensen et al. predicted that the base pair of ADA/DAD (e.g., T/N8-protonated **3**) is 11.3 kcal/mol less stable than that of DDA/AAD (e.g., C/N1-protonated **3**).[34–37]

Conclusion

A SPR sensor where a dimeric form of 2-amino-1,8-naphthyridine was immobilized was found to detect the C–C mismatch. The SPR intensity was affected by the sequence flanking to the mismatch, but clearly distinguished from that of the fully matched duplex, indicating that the sensor is potentially useful for the SNP typing in heteroduplex analyses. A modest SPR intensity and T_m increase observed for the C–T mismatch by **1** are important clues for the molecular design of drugs selectively binding to the thymine-containing mismatch.

Experimental Section

Thermal Denaturation Profiles. All UV melting experiments were carried out with a duplex containing an X–Y mismatch (4.5 μM strand) in a sodium phosphate buffer (10 mM, pH 7.0) containing NaCl (100 mM) using a SHIMADZU UV-2550 UV–vis spectrometer linked to a Peltier temperature controller. The absorbance of the sample was monitored at 260 nm from 4 to 70 °C with a heating rate of 1 °C/min in the absence and presence of a ligand.

***N*-(7-Methyl-[1,8]naphthyridin-2-yl)-propane-1,3-diamine (3).** 2-Chloro-7-methyl-1,8-naphthyridine **5** (168 mg, 0.94 mmol) was added to 1,3-diaminopropane (1.5 mL, 9.4 mmol) and stirred for 5 h at 80 °C. The solvent was evaporated, and the residue was suspended in $CHCl_3$. The organic layer was washed with 1 M NaOH, dried over $MgSO_4$, and evaporated to dryness to give **3** (196 mg, 95%) as yellow gum. ^{1}H NMR (CD_3OD, 400 MHz): δ = 7.83 (d, 1H, J = 8.0 Hz), 7.71 (d, 1H, J = 9.2 Hz), 7.01 (d, 1H, J = 8.0 Hz), 6.71 (d, 1H, J = 9.2 Hz), 3.61 (t, 2H, J = 6.8 Hz), 2.78 (t, 2H, J = 6.8 Hz), 2.55 (s, 3H), 1.84 (tt, 2H, J = 6.8 Hz J = 6.8 Hz). ^{13}C NMR ($CDCl_3$, 75 MHz): δ = 161.8, 161.5, 157.4, 138.3, 137.9, 116.6, 114.4, 39.1, 38.6, 32.5, 24.6. ESI-TOFMS calcd for $C_{12}H_{17}N_4$ [(M + H)$^+$], 217.1453; found, 217.1487.

(3,3-Diethoxy-propyl)-(7-methyl-[1,8]naphthyridin-2-yl)-amine (6). 2-Chloro-7-methyl-1,8-naphthyridine **5** (673 mg, 3.8 mmol) was added to 3,3-diethoxypropylamine (6.0 mL, 37.6 mmol) and stirred for 5 h at 80 °C. The solvent was evaporated, and the residue was suspended in $CHCl_3$. The organic layer was washed with $NaHCO_3$, dried over $MgSO_4$, and evaporated to dryness. The residue was purified by column chromatography on silica gel to give **6** (882 mg, 81%) as pale as yellow gum: ^{1}H NMR (CD_3OD, 400 MHz): δ = 7.90 (d, 1H, J = 9.0 Hz), 7.78 (d, 1H, J = 8.4 Hz), 7.06 (d, 1H, J = 7.6 Hz), 6.72 (d, 2H, J = 9.0 Hz), 4.68 (t, 1H, J = 5.6 Hz), 3.69 (q, 4H, J = 8.8 Hz), 3.59 (t, 4H, J = 6.9 Hz), 3.52 (q, 4H, J = 8.8 Hz), 2.59 (s, 3H), 1.97 (dt, 2H, J = 5.6 Hz, J = 5.6 Hz), 1.18 (t, 6H, J = 6.9 Hz). ^{13}C NMR ($CDCl_3$, 75 MHz): δ = 161.8, 161.3, 157.7, 138.3, 137.8, 118.9, 116.6, 114.3, 103.2, 62.9, 38.2, 34.5, 24.5, 15.7. HR–FABMS calcd for $C_{16}H_{24}N_3O_2$ [(M + H)$^+$], 290.1869; found, 290.1872.

***N*-(7-Methyl-[1,8]naphthyridin-2-yl)-*N'*-[3-(7-methyl-[1,8]naphthyridin-2-ylamino)-propyl]-propane-1,3-diamine (2).** To a solution of 80% AcOH–H_2O (0.5 mL) was added **5** (10 mg, 34.6 μmol). After being stirred at 60 °C for 0.5 h, triethylamine (0.9 mL), **3** (10 mg, 46.3 μmol), and sodium cyanotrihydroborate (2.2 mg, 35 μmol) were added. After being stirred for 1 h, the reaction mixture was diluted with $CHCl_3$, washed with saturated $NaHCO_3$, and dried over $MgSO_4$. The solvent was evaporated to dryness, and the residue was purified by column

(28) Calculations at the B3LYP/6-31G** level revealed that the energy gain for the formation of a hydrogen-bonding pair between 1-methylcytosine and N1-protonated 2-methylamino-7-methyl-1,8-naphthyridine is 10.9 kcal/mol, whereas that between 1-methylcytosine and nonprotonated 2-methylamino-7-methyl-1,8-naphthyridine is 4.0 kcal/mol.

(29) Binding of 2-amino-7-methyl-1,8-naphthyridine selective to the cytosine opposite the abasic site in duplex was recently reported: Yoshimoto, K.; Nishizawa, S.; Minagawa, M.; Teramae, N. *J. Am. Chem. Soc.* **2003**, *125*, 8982–8983. These authors prefer the rationalization involving two hydrogen bonds between the ligand and the cytosine. Since the N-acylated naphthyridine showed striking preference to guanine (ref 6), they assumed an additional stacking interaction that modulates the binding selectivity from G to C.

(30) Abraham, M. H. *J. Phys. Org. Chem.* **1993**, *6*, 660–684.

(31) Abraham, M. H. *Chem. Soc. Rev.* **1993**, *22*, 73–83.

(32) Beijer, F. H.; Sijbesma, R. P.; Vekemans, J. J. M.; Meijer, E. W.; Kooijman, H.; Spek, A. L. *J. Org. Chem.* **1996**, *61*, 6371–6380.

(33) Beijer, F. H.; Kooijman, H.; Spek, A. L.; Sijbesma, R. P.; Meijer, E. W. *Angew. Chem., Int. Ed. Engl.* **1988**, *37*, 75–78.

(34) Jorgensen, W. L.; Pranata, J. *J. Am. Chem. Soc.* **1990**, *112*, 2008–2010.

(35) Pranata, J. Wierschke, S. G.; Jorgensen, W. L. *J. Am. Chem. Soc.* **1991**, *113*, 2810–2819.

(36) Sartorius, J.; Schneider, H. J. *Chem.–Eur. J.* **1996**, *2*, 1446–1452.

(37) Murray, T. J.; Zimmerman, S. C. *J. Am. Chem. Soc.* **1992**, *114*, 4010–4011.

chromatography on silica gel to give **2** (14.3 mg, 12%) as pale yellow gum. ^{1}H NMR ($CDCl_3$, 400 MHz): δ = 7.73 (d, 2H, J = 8.8 Hz), 7.63 (d, 2H, J = 8.8 Hz), 6.98 (d, 2H, J = 8.0 Hz), 6.61 (d, 2H, J = 8.8 Hz), 3.72 (dt, 4H, J = 5.6 Hz, J = 5.6 Hz), 2.78 (t, 4H, J = 6.4 Hz), 2.65 (s, 6H), 1.91 (tt, 4H, J = 6.4 Hz, J = 6.4 Hz). ^{13}C NMR ($CDCl_3$, 75 MHz): δ = 161.5, 159.3, 156.7, 136.8, 136.1, 118.0, 115.0, 112.2, 40.1, 39.7, 32.4, 25.3. ESI-TOFMS calcd for $C_{24}H_{30}N_7$ [$(M + H)^+$], 416.2563; found, 416.2546.

Bis-{2-[3-(7-methyl-[1,8]naphthyridin-2-ylamino)-propylcarbamoyl]-ethyl}-carbamic Acid *tert*-Butyl Ester (7). To a solution of *N*-(*tert*-butoxycarbonyl)imino-3,3′-bis(pentafluorophenyl propionate) (198 mg, 0.33 mmol) in dry $CHCl_3$ (2 mL) were added **3** (144 mg, 0.67 mmol) and triethylamine (139 μL, 1.0 mmol). The reaction mixture was stirred at room temperature for 15 h. The solvent was evaporated to dryness, and the residue was purified by column chromatography on silica gel to give **7** (148 mg, 67%) as pale yellow solids. ^{1}H NMR (CD_3OD, 300 MHz): δ = 7.88 (d, 2H, J = 7.8 Hz), 7.76 (d, 2H, J = 8.7 Hz), 7.05 (d, 2H, J = 7.8 Hz), 6.71 (d, 2H, J = 9.0 Hz), 3.55 (t, 4H, J = 6.9 Hz), 3.51 (t, 4H, J = 6.9 Hz), 3.26 (t, 4H, J = 6.9 Hz), 2.59 (s, 6H), 2.47 (t, 4H, J = 6.9 Hz), 1.83 (tt, 4H, J = 6.9 Hz, J = 6.9 Hz), 1.40 (s, 9H). ^{13}C NMR ($CDCl_3$, 75 MHz): δ = 174.3, 162.3, 161.8, 158.1, 157.4, 138.7, 138.3, 119.4, 117.0, 114.9, 81.7, 77.9, 48.6, 46.0, 39.6, 38.4, 36.9, 36.4. ESI-TOFMS calcd for $C_{35}H_{48}N_9O_4$ [$(M + H)^+$], 658.3829; found, 658.3813.

***N*-[3-(7-Methyl-[1,8]naphthyridin-2-ylamino)-propyl]-3-{2-[3-(7-methyl-[1,8]naphthyridin-2-ylamino)-propylcarbamoyl]-ethylamino}-propionamide (1).** To a solution of **7** (76 mg, 0.133 mmol) in $CHCl_3$ (1 mL) was added ethyl acetate containing 4 M HCl (2 mL), and the reaction mixture was stirred at room temperature for 0.5 h. The solvent was evaporated to dryness to give **1** (51 mg, 80%) as white solids. ^{1}H NMR (CD_3OD, 300 MHz): δ = 7.88 (d, 2H, J = 7.8 Hz), 7.75 (d, 2H, J = 8.7 Hz), 7.05 (d, 2H, J = 7.8 Hz), 6.71 (d, 2H, J = 9.0 Hz), 3.51 (t, 4H, J = 6.9 Hz), 3.27 (t, 4H, J = 6.9 Hz), 2.86 (t, 4H, J = 6.9 Hz), 2.47 (s, 6H), 2.43 (t, 4H, J = 6.9 Hz), 1.82 (tt, 4H, J = 6.9 Hz, J = 6.9 Hz). ^{13}C NMR ($CDCl_3$, 75 MHz): δ = 175.1, 162.3, 161.8, 158.1, 138.7, 138.3, 119.4, 117.0, 114.9, 79.9, 46.8, 39.6, 38.3, 36.9, 30.5, 25.0. ESI-TOFMS calcd for $C_{30}H_{40}N_9O_2$ [$(M + H)^+$], 558.3305; found, 558.3253.

{3-[3-(Bis-{2-[3-(7-methyl-[1,8]naphthyridin-2-ylamino)-propylcarbamoyl]-ethyl}-amino)-propylcarbamoyl]-propyl}-carbamic Acid *tert*-Butyl Ester (8). To a solution of **1** (11.7 mg, 0.021 mmol) and 4-((*tert*-butoxy)carbonylamino)-*N*-(3-oxopropyl)butanamide (11 mg, 0.042 mmol) in CH_3OH (1 mL) was added sodium cyanotrihydroborate (3.3 mg, 0.05 mmol) at room temperature. The reaction mixture was kept at pH 6 with acetic acid for 1 h. The reaction mixture was diluted with $CHCl_3$, washed with saturated $NaHCO_3$, dried over $MgSO_4$, and evaporated to dryness. The residue was purified by column chromatography on silica gel to give **8** (14.3 mg, 95%) as pale yellow solids. ^{1}H NMR (CD_3OD, 400 MHz): δ = 7.85 (d, 2H, J = 8.0 Hz), 7.73 (d, 2H, J = 8.4 Hz), 7.04 (d, 2H, J = 7.6 Hz), 6.70 (d, 2H, J = 8.8 Hz), 3.54 (t, 4H, J = 6.0 Hz), 3.26 (t, 4H, J = 6.4 Hz), 3.11 (t, 2H, J = 6.8 Hz), 3.01 (t, 2H, J = 6.8 Hz), 2.74 (t, 4H, J = 6.0 Hz), 2.58 (s, 6H), 2.45 (t, 2H, J = 6.4 Hz), 2.37 (t, 2H, J = 6.4 Hz), 2.14 (t, 2H, J = 7.6 Hz), 1.81 (m, 4H), 1.70 (m, 2H), 1.60 (m, 2H), 1.40 (s, 6H). ^{13}C NMR ($CDCl_3$, 100 MHz): δ = 175.1, 169.3, 161.9, 161.3, 157.6, 138.3, 137.9, 133.6, 132.4, 129.9, 118.9, 116.6, 114.5, 79.9, 69.1, 52.0, 51.1, 40.3, 40.2, 39.3, 38.6, 34.7, 34.4, 31.6, 30.2, 28.8, 27.4, 24.9, 24.0, 14.4. ESI-TOFMS calcd for $C_{42}H_{62}N_{11}O_5$ [$(M + H)^+$], 800.4935; found, 800.4884.

1-Immobilized Sensor Surface. To a solution of **8** (1.0 mg, 1.25 μmol) in $CHCl_3$ (0.5 mL) was added ethyl acetate containing 4 M HCl (1 mL), and the reaction mixture was stirred at room temperature for 0.5 h. After evaporation of the solvent, the residue was dissolved in borate buffer (1 mL, pH 9.2) and immobilized on a sensor chip CM5 (carboxymethylated dextran surface) using amine coupling kit with a BIAcore 2000 system (BIAcore, Uppsala, Sweden). The amount of **1** immobilized on the surface was monitored as an increase of SPR signal. The change in SPR signal, termed the SPR response presented in response units (RU), is directly related to the change in surface concentration of biomolecules. SPR response of 1000 RU is equivalent to the change in surface concentration of 1 ng/mm^2. Thus, the density of immobilized ligands on the surface could be calculated by the difference in SPR response before and after the immobilization.

Acknowledgment. This work was supported by a Grant-in-Aid for Scientific Research on Priority Areas (C) "Medical Genome Science" from the Ministry of Education, Culture, Sports, Science and Technology of Japan.

JA037947W

Published online January 9, 2004

278–286 Nucleic Acids Research, 2004, Vol. 32, No. 1
DOI: 10.1093/nar/gkh171

Detection of guanine–adenine mismatches by surface plasmon resonance sensor carrying naphthyridine–azaquinolone hybrid on the surface

Shinya Hagihara[1], Hiroyuki Kumasawa[1], Yuki Goto[1], Gosuke Hayashi[1], Akio Kobori[2], Isao Saito[1] and Kazuhiko Nakatani[1,2,*]

[1]Department of Synthetic Chemistry and Biological Chemistry, Faculty of Engineering, Kyoto University, Kyoto, Japan and [2]PRESTO, Japan Science and Technology Agency (JST), Kyoto 615-8510, Japan

Received July 18, 2003; Revised October 15, 2003; Accepted November 15, 2003

ABSTRACT

We have discovered a new molecule naphthyridine–azaquinolone hybrid (Npt–Azq) that strongly stabilized the guanine-adenine (G-A) mismatch in duplex DNA. In the presence of Npt–Azq, the melting temperature (T_m) of 5′-d(CTA ACG GAA TG)-3′/3′-d(GAT TGA CTT AC)-5′ containing a single G-A mismatch increased by 15.4°C, whereas fully matched duplex increased its T_m only by 2.2°C. Npt–Azq was immobilized on the sensor surface for the surface plasmon resonance (SPR) assay to examine SPR detection of duplexes containing a G-A mismatch. Distinct SPR signals were observed when 27mer DNA containing a G-A mismatch was analyzed by the Npt–Azq immobilized sensor surfaces, whereas the signal of the fully matched duplex was ~6-fold weaker in intensity. The SPR signals for the G-A mismatch were proportional to the concentration of DNA in a range up to 1 μM, confirming that the SPR signal is in fact due to the binding of the G-A mismatch to Npt–Azq immobilized on the surface. Examination of all 16 G-A mismatches regarding the flanking sequence revealed that the sensor surface reported here is applicable to eight flanking sequences, covering 50% of all possible G-A mismatches.

INTRODUCTION

As a follow-on to the complete sequencing of the human genome, typing of single nucleotide polymorphisms (SNPs) in an array of disease-related genes is expected to be an indispensable technique for realizing personalized medicine. A number of methods have been developed for SNP typing (1–3), but much study is still needed to design new typing methods that are simple in operation, rapid and accurate in analysis, and low in cost. One of the challenges we have focused on is the reduction and eventual redundancy of labeled oligonucleotides for analysis. The expense of fluorescently labeling oligonucleotides and PCR products limits their application in large-scale typing by many currently available methods. We have reported a conceptually novel method of SNP typing that detects mismatch-containing duplexes with a small molecular ligand immobilized on a gold surface (4). Hybridization of two sets of duplex DNAs that differ from each other by a single nucleotide produces a DNA heteroduplex containing a single mismatched site. Mismatch-containing duplexes can be separated from homoduplexes by either gel electrophoresis (5,6), chemical and enzymatic cleavages at the mismatched site (7–9), or selective capture with mismatch-binding proteins (10,11). While these heteroduplex analyses applied to low-throughput screening are essentially free from oligonucleotide labeling, new technologies for high-throughput analyses are yet to be established. A small molecular ligand that selectively binds to a mismatched site could replace mismatch-binding proteins and bring an innovation to heteroduplex analyses (5,12–20). The ligand naphthyridine dimer (**Npt–Npt**) strongly and selectively binds to guanine–guanine mismatches in duplex DNA (5,12) (Fig. 1). The binding constant to a G-G mismatch in the 5′-CGG-3′/3′-GGC-5′ sequence is 1.9×10^7 M^{-1}. **Npt–Npt** consisting of two 2-amino-1,8-naphthyridine (**Npt**) chromophores, and a linker connecting the chromophores is designed so that each **Npt** produces three hydrogen bonds to each one of the guanines in the G-G mismatch, and the resultant naphthyridine–guanine pair is stabilized by stacking with the flanking base pairs. The proposed binding of **Npt–Npt** to the G-G mismatch has been verified by the 2D-NOESY spectrum of the complex (12). In addition to **Npt–Npt**, ligands that selectively and strongly bind to G-A, G-T and A-A mismatches are needed to accomplish SNP typing by a mismatch binding ligand. Taking into account the structure of **Npt–Npt** as a clue for the molecular design of ligands binding to a G-A mismatch, we have discovered naphthyridine–azaquinolone hybrids (**Npt–Azq**) where one **Npt** chromophore in **Npt–Npt** is replaced by a 8-azaquinolone chromophore (**Azq**) having complementary hydrogen-bonding surfaces to adenine (Fig. 2). Herein, we report the remarkable stabilization of G-A mismatch DNA by **Npt–Azq** and the first synthesis of a surface plasmon resonance (SPR) sensor detecting a G-A mismatch by immobilization of **Npt–Azq** on a gold surface.

*To whom correspondence should be addressed. Tel: +81 75 383 2756; Fax: +81 75 383 2759; Email: nakatani@sbchem.kyoto-u.ac.jp

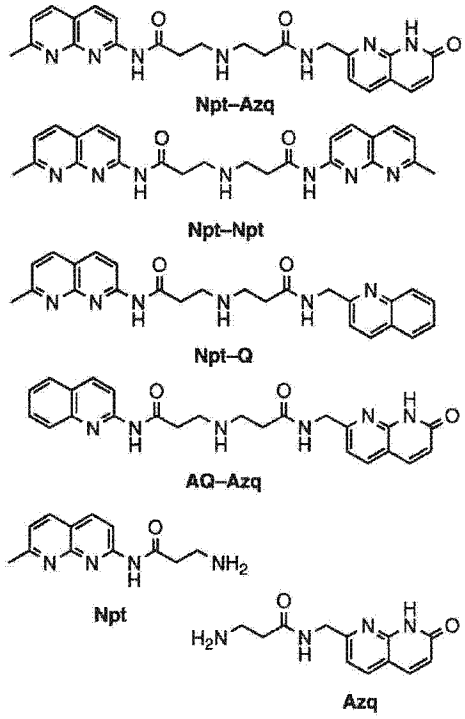

Figure 1. Formulas of **Npt**- and **Azq**-based hybrid molecules.

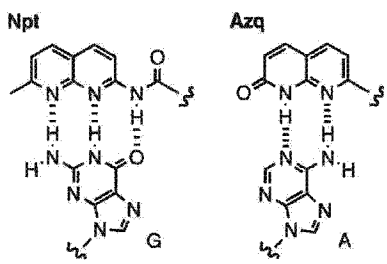

Figure 2. Hydrogen bonding patterns of **Npt**-G and **Azq**-A.

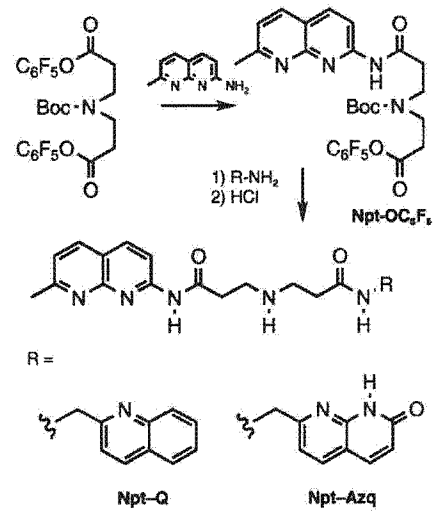

Figure 3. Synthetic scheme of **Npt**-based hybrids.

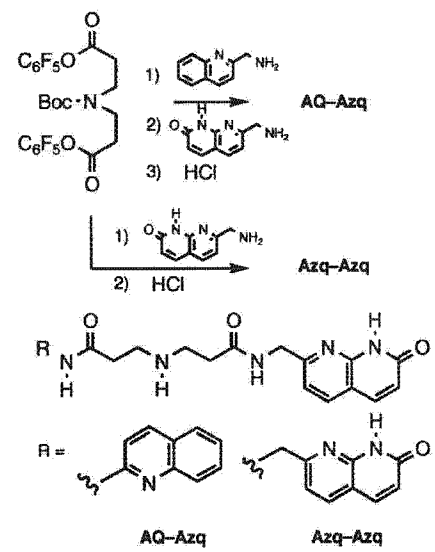

Figure 4. Synthetic scheme of **Azq**-based hybrids.

MATERIALS AND METHODS

Chemistry

In order to know the structure–activity relationship for the binding of **Npt–Azq** hybrid to G-A mismatches, hybrid molecules consisted of chromophores with different hydrogen-bonding groups were synthesized. These chromophores include **Npt**, **Azq**, quinoline (**Q**) and 2-aminoquinoline (**AQ**). Synthesis of the hybrid molecules consisting of **Npt** with **Azq** and other heterocycles is straightforward using *N*-(*tert*-butoxycarbonyl)imino-3,3′-bis(pentafluorophenyl propionate) (12), in which two carboxyl groups are activated as a pentafluorophenyl ester. Mono-substitution of the pentafluoroester with 2-amino-7-methylnaphthyridine produces intermediate amide **Npt**-OC_6F_5 that subsequently reacts with the heterocyclic amines to give hybrid ligands (Fig. 3). A similar procedure was used for the synthesis of **Azq**-based hybrid ligands (Fig. 4). Details of the synthetic procedure is described in the Supplementary Material.

Synthesis of Npt–Azq

To a solution of *N*-(*tert*-butoxycarbonyl)imino-3,3′-bis(pentafluorophenyl propionate) (1.5 g, 2.53 mmol) in dry DMF (5 ml) was added 2-amino-7-methyl-1,8-naphthyridine (180 mg, 1.14 mmol) and diisopropylethylamine (163 mg, 1.26 mmol). The reaction mixture was stirred at room temperature for 15 h. The solvent was evaporated to dryness and the residue was purified by column chromatography on silica gel to give **Npt**-OC_6F_5 (1.29 g, 90%) as pale yellow solids: ^{1}H-NMR ($CDCl_3$, 400 MHz) δ = 9.01 (br, 1H), 8.44 (d, 1H, J = 8.8 Hz), 8.12 (d, 1H, J = 8.8 Hz), 7.99 (d, 1H, J = 8.0 Hz), 7.26 (d, 1H, J = 8.0 Hz), 3.66 (m, 4H), 2.90 (m, 2H), 2.74 (m, 2H), 2.73 (s, 3H), 1.42 (s, 9H), ^{13}C-NMR ($CDCl_3$, 100 MHz) δ = 163.6, 155.3,

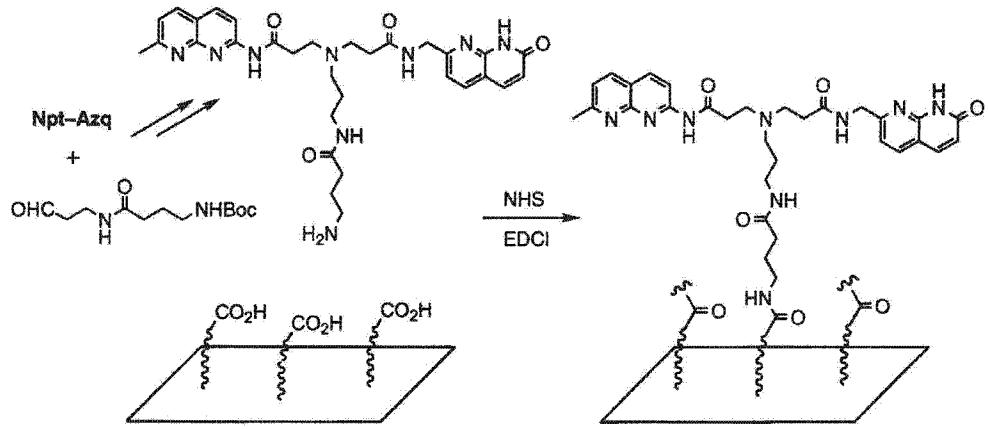

Figure 5. Synthetic scheme of **Npt–Azq** immobilized sensor surfaces.

154.6, 153.4, 142.6, 140.1, 139.5, 138.5, 136.6, 121.9, 118.8, 114.5, 80.9, 44.9, 44.4, 37.6, 37.2, 36.7, 33.4, 32.7, 28.6, 25.8, FABMS (NBA), *m/e* 569 [(M + H)$^+$], HRMS calc. for $C_{26}H_{26}O_5N_4F_5$ [(M + H)$^+$] 569.1821, found 569.1827.

To a solution of **Npt-OC$_6$F$_5$** (300 mg, 0.53 mmol) in dry DMF (2 ml) was added 7-(aminomethyl)hydro-8-azaquinolin-2-one (93 mg, 0.53 mmol) and diisopropylethylamine (77 mg, 0.6 mmol). The reaction mixture was stirred at room temperature for 15 h. The solvent was evaporated to dryness and the residue was purified by column chromatography on silica gel to give ***N*-Boc-Npt–Azq** (227 mg, 77%) as pale yellow solids: ^{1}H-NMR ($CDCl_3$, 400 MHz) δ = 11.29 (br, 1H), 9.08 (br, 1H), 8.38 (d, 1H, J = 8.8 Hz), 8.06 (d, 1H, J = 8.0 Hz), 7.95 (d, 1H, J = 8.0 Hz), 7.81 (d, 1H, J = 8.0 Hz), 7.64 (d, 1H, J = 9.6 Hz), 7.27 (d, 1H, J = 8.0 Hz), 7.22 (d, 1H, J = 8.0 Hz), 6.64 (d, 1H, J = 9.6 Hz), 4.63 (d, 2H, J = 6.0 Hz), 3.58 (t, 2H, J = 6.8 Hz), 3.57 (t, 2H, J = 6.8 Hz), 2.71 (t, 2H, J = 6.8 Hz), 2.70 (s, 1H), 2.54 (t, 2H, J = 6.8 Hz), 1.36 (s, 9H), ^{13}C-NMR ($CDCl_3$, 100 MHz) δ = 171.7, 163.9, 163.4, 159.8, 155.7, 154.5, 153.6, 149.3, 139.3, 139.2, 137.4, 136.9, 123.1, 121.9, 118.8, 118.2, 114.6, 114.0, 80.5, 44.8, 41.8, 37.5, 28.6, 25.7, FABMS (NBA), *m/e* 560 [(M + H)$^+$], HRMS calc. for $C_{29}H_{34}O_5N_7$ [(M + H)$^+$] 560.2621, found 560.2618.

To a solution of ***N*-Boc-Npt–Azq** (62 mg, 0.11 mmol) in $CHCl_3$ (3 ml) was added ethyl acetate containing 4 M HCl (2 ml) at room temperature and the reaction mixture was stirred at room temperature for 0.5 h. The solvent was evaporated to dryness to give hydrochloride of **Npt–Azq** (quantitative yield) as white solids: ^{1}H-NMR ($CDCl_3$, 400 MHz) δ = 11.45 (br, 1H), 8.67 (t, 1H, J = 5.6 Hz), 8.31 (d, 1H, J = 8.8 Hz), 7.98 (d, 1H, J = 8.8 Hz), 7.88 (d, 1H, J = 8.0 Hz), 7.65 (d, 1H, J = 7.6 Hz), 7.53 (d, 1H, J = 9.6 Hz), 7.15 (d, 1H, J = 7.6 Hz), 7.14 (t, 1H, J = 8.0 Hz), 6.58 (d, 1H, J = 9.6 Hz), 4.65 (d, 2H, J = 5.6 Hz), 3.08 (t, 2H, J = 6.0 Hz), 3.06 (t, 2H, J = 6.0 Hz), 2.65 (t, 2H, J = 6.0 Hz), 2.58 (t, 2H, J = 6.0 Hz), 2.57 (s, 3H), ^{13}C NMR (CD_3OD, 100 MHz) δ = 171.8, 171,3, 165.0, 160.2, 159.7, 157.0, 148.5, 147.3, 146.4, 140.3, 140.2, 138.8, 122.5, 120.9, 120.2, 117.6, 117.0, 114.8, 44.1, 43.9, 43.1, 32.5, 30.5, 19.7, FABMS (NBA), *m/e* 460 [(M + H)$^+$], HRMS calc. for $C_{24}H_{26}O_3N_7$ [(M + H)$^+$] 460.2095, found 460.2097.

Synthesis of Npt–Azq having an aminoalkyl linker for immobilization onto SPR sensor surface

SPR sensors having **Npt–Azq** on their surface were synthesized to examine SPR detection of the G-A mismatch in a flow system (Fig. 5). **Npt–Azq** was immobilized on a dextran matrix coated gold surface (CM5 chip, BIAcore) through a bivalent linker of *N*-Boc-aminoaldehyde. First, **Npt–Azq** was tethered by a reductive amination to the linker, which was efficiently prepared from Boc-protected 4-aminobutanoic acid and 3-aminopropionaldehyde diethylacetal (Supplementary Material). Deprotection of a Boc group produced a primary amine, which was subsequently immobilized on the sensor surface by a coupling between the amino group and an activated carboxyl group on the CM5 chip using a standard method with 1-(3-dimethylaminopropyl)-3-ethylcarbodiimide hydrochloride (EDCI) and *N*-hydroxysuccinimide (NHS).

Preparation of a sensor chip carrying Npt–Azq on its surface

SPR measurements were performed with a BIAcore 2000 system (BIAcore, Uppsala, Sweden). Immobilization of **Npt–Azq** on a sensor chip CM5 (carboxymethylated dextran surface, BIAcore) was carried out using amine coupling kit (BIAcore) in a continuous flow of HBS-N buffer (10 mM HEPES, pH 7.4) containing NaCl (150 mM) at a flow rate of 10 µl/min. A solution (70 µl) of NHS (0.05 M) and EDCI (0.2 M) was injected using the QUICKINJECT command to activate the carboxymethylated dextran surface of a CM5 sensor chip. A solution (70 µl) of **Npt–Azq** having an aminoalkyl linker (2 mM in borate buffer, pH 9.2) was injected using the QUICKINJECT command on the activated surface. Residual activated surface was completely blocked by injection of a solution (20 µl) of ethanolamine hydrochloride (1.0 M, pH 8.5). Non-covalently bound material was removed by washing with 5 µl of 50 mM NaOH to produce the sensor chip carrying **Npt–Azq** on its surface. The amount of **Npt–Azq** immobilized on the surface was modulated by the reaction period of the immobilization, and was monitored as an increase of SPR signal [resonance unit (RU)] after the deactivation of the unreacted NHS-esters and a conditioning

Table 1. ΔT_m values for the duplexes containing **G-y** mismatches in the absence and presence of drugs[a]

Drug	**cGg/gAc**, T_m = 25.8°C	**cGg/gGc**, T_m = 25.1°C	**cGg/gCc**, T_m = 38.6°C
Npt–Azq	15.4 (0.6)	10.6 (0.7)	2.2 (0.8)
Npt–Npt	12.8 (1.0)	26.2 (1.0)	4.3 (1.0)
Npt–Q	1.6 (1.5)	4.5 (1.3)	2.0 (1.0)
AQ–Azq	–0.4 (0.4)	0.1 (0.1)	0.7 (0.4)
Azq–Azq	–0.5 (0.1)	–0.9 (0.7)	0.5 (0.6)
Npt	–0.6 (0.4)	–0.8 (0.2)	–0.3 (0.7)
Azq	0.3 (0.3)	0.3 (0.6)	0.4 (1.0)
Npt and **Azq**	–0.6 (0.5)	–0.8 (0.5)	–0.2 (0.1)

[a]T_m for the duplex 5′-d(CTAA **vGw** AATG)-3′/3′-d(GATT **xyz** TTAC)-5′ (5.0 μM each strand) in the absence (drug –) and presence (drug +) of drug (200 μM) was measured in 10 mM sodium cacodylate buffer (pH 7.0) containing 100 mM NaCl. $\Delta T_m = T_m$ (drug +) – T_m (drug –). The numbers in parentheses represent the maximum experimental error.

of the surface. Three sensor surfaces carrying **Npt–Azq** for 527, 722 and 951 RU were obtained by the immobilization for 1, 3 and 7 min with a 2 mM solution of **Npt–Azq** in a borate buffer (pH 9.2).

Measurements of thermal denaturation profiles of mismatch-containing duplexes

Thermal denaturation profiles of the duplexes 5′-d(CTAA **vGw** AATG)-3′/3′-d(GATT **xyz** TTAC)-5′ where G-**y** mismatches were flanked by **v-x** and **w-z** base pairs (4.5 or 5.0 μM for each strand) were measured in a sodium cacodylate buffer (10 mM, pH 7.0) containing NaCl (100 mM) using a Shimadzu UV-2550 UV-Vis spectrometer linked to a Peltier temperature controller. The absorbance of the sample was monitored at 260 nm from 4 to 70°C with a heating rate of 1°C/min in the absence and presence of a hybrid ligand. The measurements were carried out at the ligand concentration of 50 or 200 μM. The melting temperature of these duplexes was determined as the temperature crossing the melting curve and the median of two straight lines drawn for the single and duplex region in the melting curve.

General procedure for SPR binding experiments using synthetic oligonucleotides

All measurements were carried out at 25°C in a continuous flow of a buffer (10 mM HEPES, pH 7.4) containing NaCl (1 M) at a flow rate of 30 μl/min. A 1 μM solution of 27mer duplexes 5′-d(GTT ACA GAA TCT **VGW** AAG CCT AAT ACG)-3′/3′-d(CAA TGT CTT AGA **XYZ** TTC GGA TTA TGC)-5′ containing G-Y mismatches flanked by V-X and W-Z base pairs in the buffer were injected for 180 s for analyzing the association to the sensor surface. The buffer was subsequently injected for another 180 s for analyzing the dissociation of the bound oligomer form the surface. After each analysis, all binding materials were removed by washing with 30 μl of NaOH solution (50 mM). Immediately after washing, this system can be used for the next assay.

RESULTS AND DISCUSSION

UV melting temperature analyses

The bindings of **Npt–Azq** and other hybrid ligands to G-**y** mismatches were examined by measuring the melting temperature (T_m) of mismatch-containing duplexes (5.0 μM) in the presence of the ligand. The difference of the melting temperature (ΔT_m) in the absence and presence of the ligands is summarized in Table 1. A large ΔT_m of 26.2°C was obtained for the 11mer duplex containing the G-G mismatch flanked by two G-C base pairs (**vGw/xyz** = **cGg/gGc**) in the presence of **Npt–Npt**. In order to distinguish the 11mer duplexes used for the T_m measurements from the 27mer duplexes used for SPR studies, the flanking sequences to the mismatch of 11mer were described with lowercase letters, whereas uppercase letters were used of the flanking sequences of 27mer. Under these conditions, **Npt–Npt** also increased the T_m of the G-A mismatch (**cGg/gAc**) by 12.8°C, whereas only a modest ΔT_m of 4.3°C was observed for the matched duplex. In contrast to **Npt–Npt**, substitution of one **Npt** chromophore to **Azq** in **Npt–Azq** showed a striking difference in the spectrum for mismatch stabilization. **Npt–Azq** strongly stabilizes **cGg/gAc** as indicated by the ΔT_m of 15.4°C, exceeding the ΔT_m of **Npt–Npt** by 2.6°C. Since the non-specific binding to a fully matched duplex is weaker for **Npt–Azq** (2.2°C) than **Npt–Npt** (4.3°C), **Npt–Azq** is currently the strongest ligand described that stabilizes the G-A mismatch.

To gain insight into a role of **Azq** chromophore for the binding to the G-A mismatch, the **Azq** and **Npt** chromophores in **Npt–Azq** were replaced by either quinoline (**Q**) or aminoquinoline (**AQ**) chromophores. A dramatic decrease of the ΔT_m from 15.4 to 1.6°C was observed by replacing **Azq** chromophore in **Npt–Azq** with **Q** in **Npt–Q**. The hydrogen-bonding donor of N-H in **Azq** was replaced by a non-hydrogen bonding group of C-H. Aminoquinoline–azaquinolone (**AQ–Azq**) obtained by a substitution of **Npt** in **Npt–Azq** with **AQ** completely lost the binding to both G-A and G-G mismatches (Fig. 6). Furthermore, the azaquinolone dimer (**Azq–Azq**), the single chromophore **Npt** and **Azq**, or the 1:1 mixture of **Npt** and **Azq** did not stabilize the G-A mismatch. These results clearly indicated that a covalent attachment of **Npt** and **Azq** chromophores is essential for the stabilization of the G-A mismatch. These remarkable effects of the substitution of the **Npt** and **Azq** chromophores in **Npt–Azq** on the stabilization of the G-A mismatch suggests the significance of the hydrogen bonding of **Azq** to adenine and **Npt** to guanine (Fig. 2). It has been recently shown that **Azq** is superior to thymine in the recognition of adenine in duplex and triplex structure (21). These observations are well consistent to our results.

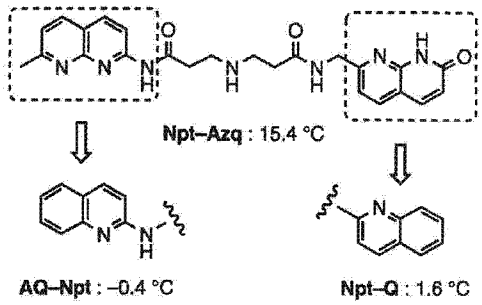

Figure 6. Schematic representation of the effect of structural modification of chromophores in **Npt–Azq** on the increased melting temperature (ΔT_m) of the G-A mismatch.

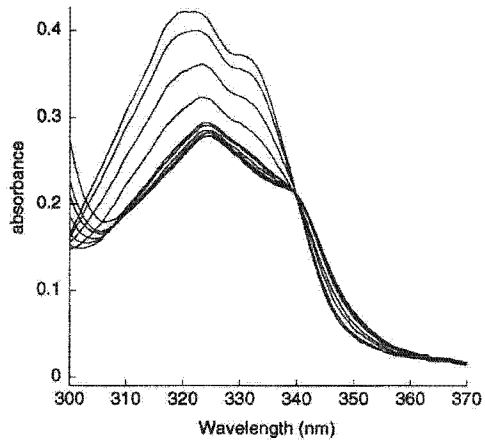

Figure 7. UV absorption spectra of **Npt–Azq** (20 μM) in the presence of different concentrations of the G-A mismatch duplex **cGg/gAc** (0–50 μM). The experiments were conducted in a sodium cacodylate buffer (10 mM, pH 7.0) containing NaCl (100 mM) at 15°C. The concentrations of DNA are 0, 1, 2.5, 5, 7.5, 10, 15, 20, 25 and 37.5 μM.

Evaluation of the binding of Npt–Azq to G-A mismatches

Having found that **Npt–Azq** strongly stabilizes the G-A mismatch, and that the hydrogen bonding groups in the two chromophores are essential, the binding of the ligand was studied in detail. First, the UV absorption of the **Npt–Azq** (20 μM) was measured in the presence of different concentrations of the 11mer G-A mismatch duplex (**cGg/gAc**) (0–50 μM). In the absence of DNA, the ligand showed an absorption maximum at 320 nm and a shoulder at 333 nm. At increasing **cGg/gAc** concentrations, these absorptions decreased in intensity with a concomitant red shift of the peak from 320 to 324 nm (Fig. 7). An isosbestic point was observed at 340 nm for the spectral change, indicating that UV absorbance of **Npt–Azq** linearly changes from the free state to the bound state to **cGg/gAc**. With the data points at 320 nm, the fraction of the total ligand bound against the molar fraction of **cGg/gAc** ([**cGg/gAc**] / [**Npt–Azq**]) was plotted (Fig. 8). The bound fraction of **Npt–Azq** rapidly increased with increasing **cGg/gAc** concentration and saturated in the presence of approximately one molar equivalent of DNA. In contrast, the bound fraction of **Npt–Npt** to the G-A mismatch

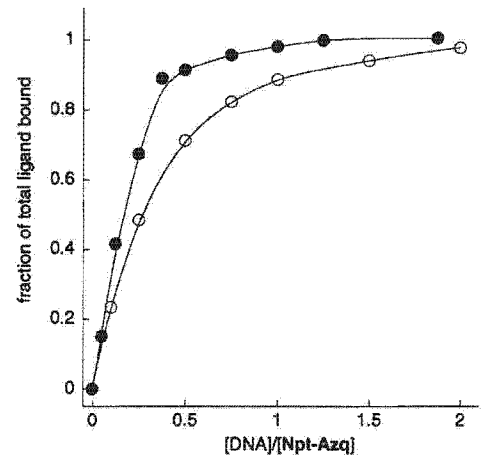

Figure 8. Plot of the fraction of total ligand bound against the molar fraction of the G-A mismatch duplex **cGg/gAc** to the concentration of **Npt–Azq** (filled circles) and **Npt–Npt** (open circles), respectively. The data were obtained from experiments shown in Figure 7.

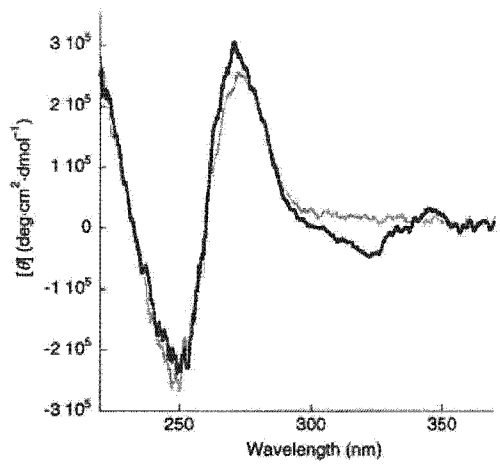

Figure 9. CD spectra of **cGg/gAc** (4.5 μM) measured in 10 mM sodium cacodylate buffer (pH 7.0) and 100 mM NaCl at 25°C in the absence (gray) and presence (black) of 20 μM **Npt–Azq**.

steadily increased with increasing **cGg/gAc** concentration and reached saturation with two molar equivalents of DNA. This suggests that the binding of **Npt–Azq** to the G-A mismatch is stronger than that of **Npt–Npt**. CD spectra of **cGg/gAc** in the presence of **Npt–Azq** showed an increase of the ellipticity at 275 nm in addition to strong and weak CD signals induced at 320 and 345 nm, respectively (Fig. 9). Distinct induced CD signals indicated that **Npt–Azq** was under the influence of the chiral environment of duplex DNA in the complex.

The effect of the concentration of **Npt–Azq** on the ΔT_m of **cGg/gAc** was examined by measuring the melting curve at different drug concentrations. Increasing the concentration of **Npt–Azq**, the ΔT_m of the duplex increased and reached a plateau (Fig. 10). At 50 μM **Npt–Azq**, UV-melting profiles were obtained for all G-A mismatches with regard to the sequence flanking to the mismatch (**vGw/xAz**). The T_m of all G-A mismatches except for **tGt/aAa** in the absence and

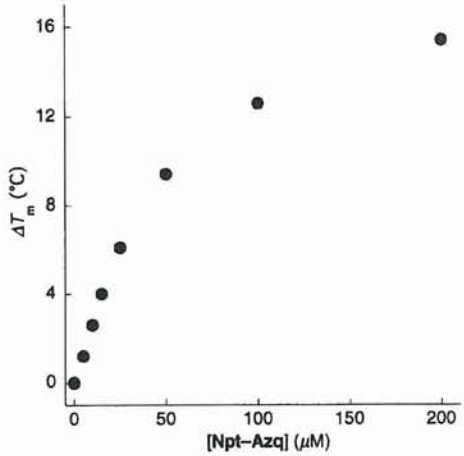

Figure 10. Concentration dependency of ΔT_m of **cGg/gAc** (4.5 μM). The melting temperature of **cGg/gAc** (4.5 μM) was measured in the presence of 0, 5, 10, 15, 25, 50, 100 and 200 μM **Npt–Azq** in 10 mM sodium cacodylate (pH 7.0) and 100 mM NaCl.

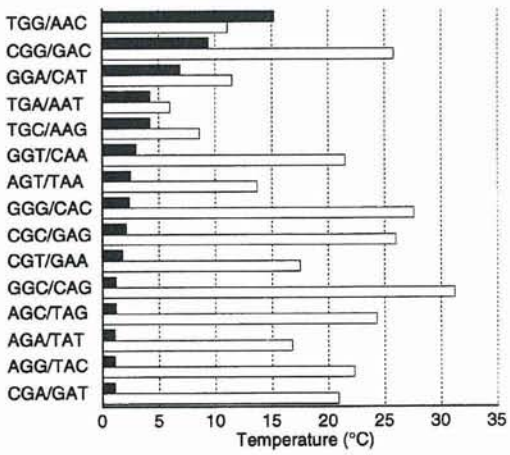

Figure 11. ΔT_m values for G-A mismatches (4.5 μM) of different flanking sequence in the presence of **Npt–Azq** (50 μM) (black) and melting temperatures of G-A mismatches in the absence of **Npt–Azq** (white).

presence of **Npt–Azq** are summarized in Figure 11. The T_m of **tGt/aAa** was too low to measure under the conditions. The largest ΔT_m was recorded for the sequence of **tGg/aAc**. The sequence **cGg/gAc** we have examined in detail had the second largest ΔT_m value. While we have anticipated that the binding of **Npt–Azq** would be favorable for the G-A mismatches flanking to G-C base pairs due to the increased stacking stabilization of the complex, there seems no obvious rationalization for the sequences stabilized by the drug. The melting curves of the sequences showing the top five ΔT_m values are shown in Figure 12. The energy gains of these five G-A mismatches in the presence of 50 μM **Npt–Azq** were estimated by curve fitting of the melting profiles. The melting profile of the G-A mismatch in the absence and presence of **Npt–Azq** were fitted to a two-state model with a non-linear least-squares program by using Sigma Plots (version 2001) (22). The energy gains obtained by these simulations are

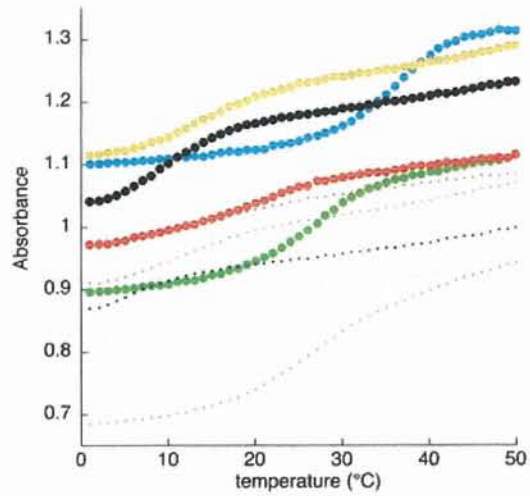

Figure 12. Melting curves of G-A mismatch duplexes (4.5 μM) in the absence (dots) and presence (filled circles) of **Npt–Azq** (50 μM) in 10 mM sodium cacodylate (pH 7.0) and 100 mM NaCl. **tGg/aAc**, green; **cGg/gAc**, blue; **gGa/cAt**, red; **tGc/aAg**, orange; **tGa/aAt**, black.

Table 2. Estimated energy gains of the G-A mismatches in the presence of 50 μM **Npt–Azq**[a]

G-A mismatch	ΔG (drug –)	ΔG (drug +)	$\Delta\Delta G$
cGg/gAc	–9.7	–15.7	–6.0
tGc/aAg	–10.5	–14.6	–4.1
tGg/aAc	–8.4	–12.1	–3.6
gGa/cAt	–6.0	–8.9	–2.9
tGa/aAt	–8.1	–9.8	–1.7

[a]ΔG (drug –) and ΔG (drug +) were obtained by curve fitting of the melting profiles in the absence and presence of **Npt–Azq** (50 μM) at 277.15 K and reported in kcal/mol. $\Delta\Delta G = \Delta G$ (drug +) – ΔG (drug –).

summarized in Table 2. The largest energy gain of –6.0 kcal/mol (277.15 K) was obtained for **cGg/gAc**, whereas the sequence **tGg/aAc**, which recorded the highest ΔT_m value, was ranked third. As we reported earlier, the magnitude of ΔT_m is not consistent with the energy gain by the drug binding especially when the duplex showed a low melting temperature (23).

SPR analyses

Having discovered that **Npt–Azq** strongly stabilizes the G-A mismatch DNA, the binding of G-containing mismatches to the SPR sensor where **Npt–Azq** was immobilized on the surfaces was investigated. SPR analyses of a 1 μM solution of 27mer duplexes 5′-d(GTT ACA GAA TCT **VGW** AAG CCT AAT ACG)-3′/3′-d(CAA TGT CTT AGA **XYZ** TTC GGA TTA TGC)-5′ containing a G-Y mismatch flanked by G-C base pairs (5′-**VGW**-3′/3′-**XYZ**-5′ = CGG/GYC, Y = A, G or C) were performed with the sensor carrying **Npt–Azq** for 951 RU on the surface. To suppress a non-specific absorption of DNA to the sensor surface, binding experiments were carried out under high salt conditions (1 M NaCl and 10 mM HEPES buffer, pH 7.4). A sensorgram obtained for the G-A mismatch (**CGG/GAC**) showed strong SPR signals, of which intensity reached to 193 RU, after 180 s of the association time

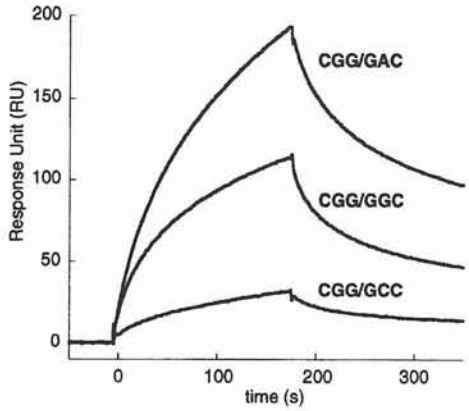

Figure 13. Sensorgrams for the binding of duplexes containing G-Y mismatches to the **Npt–Azq** immobilized SPR sensor surface. Aliquots of 90 µl of the duplexes (1.0 µM in 10 mM HEPES buffer pH 7.4, 1 M NaCl) containing G-A, G-G mismatch and G-C matches were injected for 180 s to measure the association to the sensor surface.

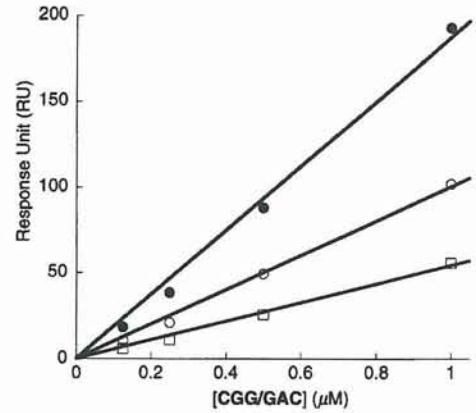

Figure 14. Concentration dependency for the SPR responses for 27mer duplex (**CGG/GAC**) containing a G-A mismatch. **CGG/GAC** at concentrations of 0.13, 0.25, 0.5 and 1.0 µM were analyzed by three sensors carrying **Npt–Azq** for 951 (filled circles), 722 (open circles) and 527 RU (squares) on the surface. Responses after 180 s of the association time were plotted against the DNA concentration.

(Fig. 13). The SPR signal for the G-G mismatch (**CGG/GGC**) was also distinct, but much lower in intensity (114 RU) than that obtained for **CGG/GAC**. In marked contrast, only a weak SPR signal (31 RU) was observed for the G-C match DNA (**CGG/GCC**). These results are consistent with those of UV-melting studies in the presence of **Npt–Azq** showing a higher ΔT_m for **cGg/gAc** than for **cGg/gGc** and almost negligible stabilization for the G-C match DNA. The distinct differences in the intensity of the SPR signal between the G-A mismatch and G-C match DNA clearly indicate a unique character of the **Npt–Azq** immobilized sensor surface.

Concentration dependency for the SPR responses

To further evaluate the fidelity of the novel sensor surfaces detecting the G-A mismatches, the concentration dependency of the SPR signal for the binding of the G-A mismatch to the sensor surface was investigated. The duplex **CGG/GAC** containing a G-A mismatch of different concentrations (0.13–1.0 µM) was analyzed by three sensor surfaces carrying **Npt–Azq** for 951, 722 and 527 RU. The SPR responses after the association time of 180 s were plotted against the concentration of the G-A mismatch DNA (Fig. 14). The SPR signals produced by each sensor surface clearly showed a linear correlation to the concentration of **CGG/GAC**, with a correlation coefficient of 0.99. A linear correlation between SPR intensity and DNA concentrations validated that the observed SPR signals were definitely due to a specific interaction between **CGG/GAC** and **Npt–Azq** on the sensor surface. Furthermore, it was suggested that the sensor surface is not only effective to detect the G-A mismatch, but also applicable to quantify G-A mismatch DNA at the concentration range up to 1 µM (24). It is worth noting that the SPR responses of three sensor surfaces were not proportional to the amount of **Npt–Azq** immobilized on the surface. This is most likely due to the different surfaces of the three sensors produced by independent immobilization processes for the three CM5 chips of research grade. Thus, calibration of the sensor surface is necessary for quantitative applications.

Effect of the flanking sequence to the G-A mismatch on the SPR responses

To know the scope and limitation of the novel G-A mismatch detecting sensor, the effect of the sequence flanking to the mismatch on the binding to the **Npt–Azq** immobilized sensor surface was examined. In heteroduplex analyses, it is important to differentiate the mismatch-containing duplex from the fully matched duplex. Thus, the SPR signal of a mismatched duplex relative to that of the fully matched duplex was investigated. DNA duplexes containing G-A mismatches in the sequence of 5′-**VGW**-3′/3′-**XAZ**-5′ were analyzed by SPR using an **Npt–Azq** immobilized sensor surface. SPR intensities of 16 G-A mismatches were reported by the relative intensity to the highest signal of the fully matched duplex. G-A mismatches are largely divided into three groups with regard to the affinity to the surface. The first group of G-A mismatches showed a strong response to the **Npt–Azq** immobilized surfaces. Among 16 duplexes, the strongest SPR signal was observed for **TGG/AAC** (Fig. 15a). The SPR intensity was more than two times stronger than the signal for **CGG/GAC**, and 12-fold stronger than that observed for the matched duplex. Besides these two, G-A mismatches in **GGA/CAT**, **TGC/AAG**, **AGG/TAC** and **AGA/TAT** showed SPR signals that are markedly stronger than the signal of a matched duplex by >2-fold. The fitting of the response curve to a 1:1 Langmuir model with BIAevaluation software (version 3) provided an estimate of the association constant (K_a) of each G-A mismatch to the **Npt–Azq** immobilized surface. The K_a obtained for the G-A mismatches were 1.8×10^6 M^{-1} for **TGG/AAC**, 1.0×10^6 M^{-1} for **CGG/GAC**, 9.0×10^5 M^{-1} for **GGA/CAT**, 9.2×10^5 M^{-1} for **AGG/TAC** 7.5×10^5 M^{-1} for **AGA/TAT**. The K_a for the **TGC/AAG** could not be estimated due to a very slow dissociation of DNA from the surface. The second group of G-A mismatches showed reduced relative intensities compared with those in the first group (Fig. 15b). The SPR responses of **AGT/TAA** and **GGG/CAC** are clearly distinguished from that of matched duplex. The relative intensity of the SPR signal to the mismatches is ~1.5-fold. The